JOURNAL OF THEORETICAL AND APPLIED MECHANICS
50, 2, pp. 509-530, Warsaw 2012
50th Anniversary of JTAM

THE MODELLING OF LOADING, UNLOADING AND RELOADING OF THE ELASTIC-PLASTIC CONTACT OF ROUGH SURFACES

Robert Kostek

University of Technology and Life Science in Bydgoszcz, Faculty of Mechanical Engineering, Bydgoszcz, Poland; e-mail: robertkostek@o2.pl

This paper presents a non-linear mathematical model describing the hysteresis of dry contact of rough surfaces loaded in the normal direction. A number of characteristic phenomena appear during the initial loading, unloading and reloading of the contact interface. The contact is most flexible during the first loading, and its plastic deflection is significant, whereas the characteristic curve of unloading is stiffer and is mainly elastic in nature. The reloading characteristic is similar to the unloading characteristic, and thus a hysteresis loop is observed. The non-linear model of contact presented in this paper, which has been validated by experimental data, describes the aforementioned phenomena. The model is dedicated to the finite element method (FEM), the discrete element method (DEM), and simulations of multi-body systems (MBS), where accurate and effective contact models are preferred. The presentation of the model is supported by examples of applications to contact problems.

Key words: contact model, elastic-plastic, rough surface, hysteresis

1. Introduction

Contact interfaces often exist in machines (e.g., sideways). The contact interfaces operate under dynamic loading and are thus repeatedly loaded and unloaded. Contact deflections are particularly important in the case of precision machines, such as machine tools, measuring equipment and microscopes.

The specific physical phenomena that occur at the contact of two rough surfaces are strongly non-linear. The maximum normal force influences the residual deflection of the contact (Etsion *et al.*, 2005; Kadin *et al.*, 2006). The plastic deflection of a virgin contact is significant (Goerke and Willner, 2008;

Tworzydlo *et al.*, 1998; Vu-Quoc and Zhang, 1999), whereas a stabilised contact is stiffer, and its deflection is mostly elastic in nature (Skrodzewicz, 2003). Moreover, the hysteresis loops of stabilised contact joints are not very sensitive to the frequency of external forces, within the frequency range 0.1-2400 Hz (Gutowski and Skrodzewicz, 2001; Kostek, 2005). The specific phenomena make it difficult to model the contact; thus, contact models are dedicated to specific applications. In tribology, accurate and complex models are preferred. They are based on statistical modelling (Kadin *et al.*, 2006), fractal theory (Goerke and Willner, 2008; Pei *et al.*, 2005), FEM (Tworzydlo *et al.*, 1998; Pei etal, 2005), and modelling dislocations within crystals (Nicola etal, 2007). Analysis of these models provides valuable information, but simulations using such models are computationally expensive. In contrast, simple and fast models based on linear (Kruggel-Emden etal, 2008; Munjiza, 2004) and non-linear formulae (Grudziński and Kostek, 2007; Hess and Soom, 1991; Hunt and Crossley, 1975; Kostek, 2005; Kruggel-Emden etal, 2008; Martins etal, 1990; Michalczyk, 2008; Pombo and Ambrósio, 2008; Schiehlen etal, 2006) are preferred in computational mechanics and dynamics. These models are usually used to describe collisions between bodies, vibrations, pressure distributions and restitution coefficients, which are coupled with the contact phenomena (see, e.g., Lifshitz and Kolsky, 1963; Oden and Martins, 1985; Wriggers, 2006).

The contact interfaces of rough surfaces have been investigated by researchers, and contact models describing loading and unloading seem to be the most valuable. Tworzydlo *et al.* (1998) presented asperity-based constitutive models of contact interfaces. Skrodzewicz (2003) presented non-linear mathematical models describing hysteresis loops of stabilised contacts loaded by harmonic forces. Kim *et al.* (2004) worked on ultrasonic experiments characterised by the elasto-plastic planar contact. Jones (2004) presented a model of a rough surface with columnar and spherical asperities. Pei *et al.* (2005) presented an FEM study of the contact between a rigid plane and an elasto-plastic solid with a self-affine fractal surface. Kadin *et al.* (2006) presented a statistical model of the unloading of the elasto-plastic contact of rough surfaces. Goerke and Willner (2008) worked on a numerical model that describes the elasto-plastic normal contact of isotropic fractal surfaces. Kostek and Konowalski (2008) presented a non-linear model describing the loading and unloading contact of two rough surfaces.

Several articles have addressed elasto-plastic Hertzian contact in the Greenwood-Williamson model (Archard, 1957; Etsion *et al.*, 2005; Greenwood and Williamson, 1966; Jamari and Schipper, 2007; Li and Gu, 2009; Pullen and Williamson, 1972; Schiehlen *et al.*, 2006; Vu-Quoc and Zhang, 1999; Woo

and Thomas, 1980), which can be relevant to the contact of asperities. Thus, these articles have been mentioned in this paper.

As is evident from the literature search, there are many models of contact. However, a model that has been validated by experimental data and that is able to precisely describe the initial loading, unloading and reloading in the normal direction of a planar contact of rough surfaces has not been found. Thus, there is a need to present a suitable model for that case.

2. Formulation of the mathematical model

The interface of two bodies in a planar contact, which is shown in Fig. 1a, is modelled in this Section. The interface can be modelled with a large number of springs and plastic bodies (Saint-Venant elements) (Fig. 1b), which represent interacting roughness asperities. It is assumed that the mechanical properties of the contact interface are macroscopically identical over the entire contact area. Thus, after homogenisation (Fig. 1c), the contact zone can be modelled as

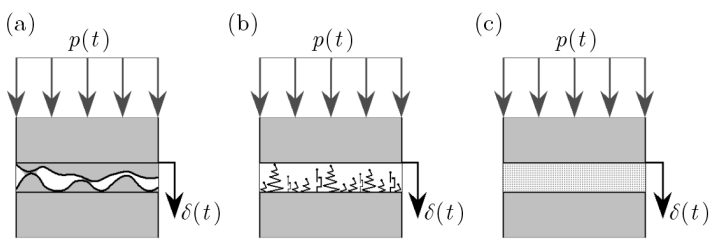

Fig. 1. Schematic of the contact interface (a) and its physical models (b), (c)

a homogenous area that possesses specific elasto-plastic properties. Deflection of the contact zone can be expressed as a function of loading, where the input signal is the normal contact pressure p, and the output signal is the contact deflection δ. The experimental and analytical investigations presented previously (Mikic, 1971, 1974; Tworzydlo *et al.*, 1998) show that the interactions within a dry contact exhibit elastic, plastic and elasto-plastic nature (Fig. 2d), and thus the contact model consists of three elements (Fig. 2a). The elastic normal deflection is described by equation $(2.1)_1$ (Martins *et al.*, 1990), and the plastic normal deflection is expressed by similar equation $(2,1)_2$ as follows

$$\delta_e = e_e p^{m_e} \qquad \delta_p = e_p p_{max}^{m_p} \tag{2.1}$$

where δ_e denotes the normal elastic deflection of the interface, δ_p represents the normal plastic deflection of the interface, p is the normal contact pressure,

p_{max} is the maximum normal contact pressure for a specified period of time $p_{max} = \max(p_0, p_1, p_2, \ldots, p_n)$, and e_e, e_p, m_e and m_p are the parameters of the interface. The non-linear elastic element models the reversible part of the contact deflection, whereas the non-linear plastic element models the irreversible part of the contact deflection. The most important feature of the elastic element is that its deflection does not depend on the previous loading history, only on the present contact pressure p, whereas the plastic element deflection is determined by the maximum magnitude of the loading pressure p_{max}. The plastic contact deflection increases only if the maximal contact pressure p_{max} increases. The two elements are able to describe pure elastic and pure plastic deflections (Kostek and Konowalski, 2008; Nardin *et al.*, 2003).

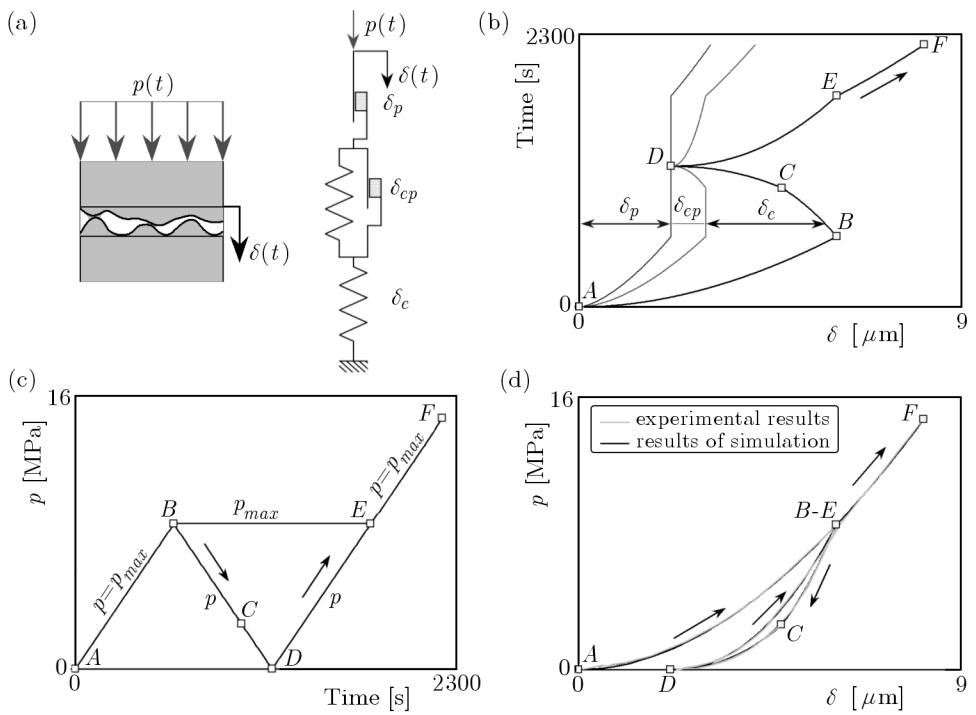

Fig. 2. A load-deflection characteristic (d) of the contact model (a) obtained for the presented input (c) and output signals (b) and validated against experimental results (see Tworzydlo *et al.*, 1998; Fig. 20a)

The application of the elasto-plastic element provides an opportunity to model the hysteresis of a preloaded contact and the dissipation of energy within this type of contact. This element can be modelled as a parallel connection of the elastic and plastic bodies (Fig. 3 a), described by equations (2.2). The pla-

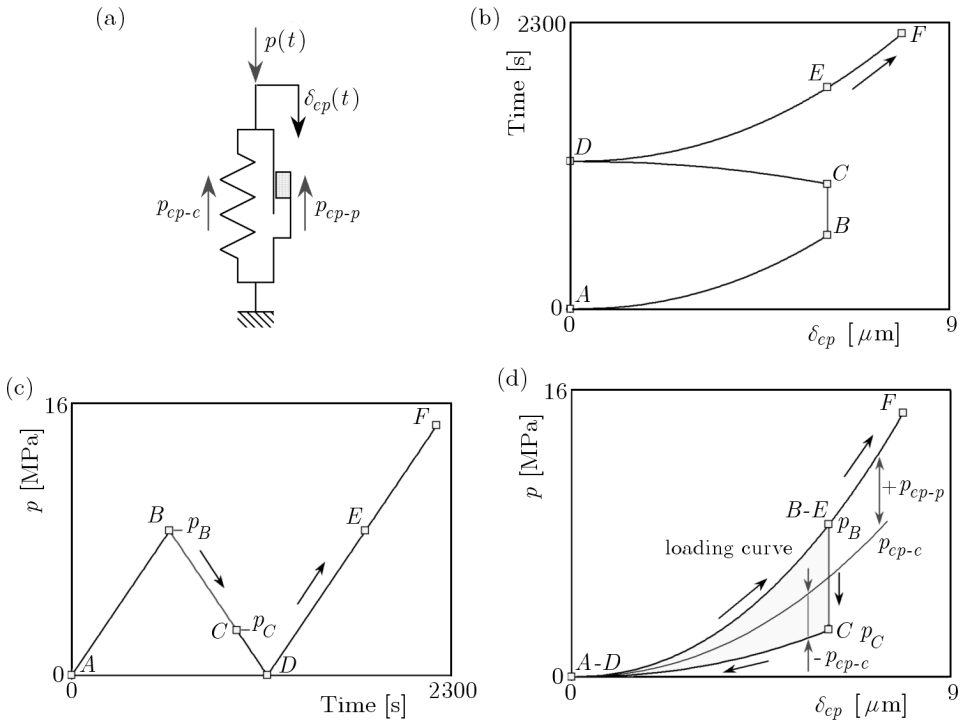

Fig. 3. A load-deflection characteristic (d) of the elasto-plastic element (a) obtained for the presented time histories (b), (c)

stic body models the dissipation of energy and damping, and thus its pressure is related to the sign of its velocity of deflection. It should be mentioned here that the damping pressure is insensitive to the magnitude of the speed, which reflects the plastic nature of dissipation energy. In general, the elasto-plastic element is described by the following equations

$$p_{ep-e} = \Big(\frac{\delta_{ep}}{e_{ep-e}}\Big)^{1/m_{ep-e}} \qquad p_{ep-p} = \operatorname{sgn}\Big(\frac{d\delta_{ep}}{dt}\Big)\Big(\frac{\delta_{ep}}{e_{ep-p}}\Big)^{1/m_{ep-p}} \tag{2.2}$$

and

$$p(t) = p_{ep-e} + p_{ep-p} = \Big(\frac{\delta_{ep}}{e_{ep-e}}\Big)^{1/m_{ep-e}} + \operatorname{sgn}\Big(\frac{d\delta_{ep}}{dt}\Big)\Big(\frac{\delta_{ep}}{e_{ep-p}}\Big)^{1/m_{ep-p}} \tag{2.3}$$

where δ_{ep} denotes the normal elasto-plastic deflection of the interface, p_{ep-e} is the normal contact pressure in the elastic element, p_{ep-p} is the normal contact pressure in the plastic element, t is time, and e_{ep-e}, e_{ep-p}, m_{ep-e} and m_{ep-p} are interface parameters. In this case, the input signals are δ_{ep} and $d\delta_{ep}/dt$,

whereas the output signal is the normal contact pressure p. First, during the initial loading from point A to point B, both p_{ep-e} and p_{ep-p} are positive ($d\delta_{ep}/dt > 0$), and thus these two elements act against the normal contact pressure p. In consequence, the elasto-plastic element follows the loading curve (Fig. 3d). Next, the unloading from point B to C does not change the deflection of the elastic element ($d\delta_{ep}/dt = 0$) (Fig. 3b,d), but only changes the normal contact pressure in the plastic element p_{ep-p}, which is because the plastic element stops the changes of deflection, which is typical for systems with dry friction. The contact pressure during this period drops from p_B to p_C, due to a drop of the external force. The contact pressure being in the range from p_C to p_B is not able to change the deflection of the elastic element. Then, the unloading from point C to point D reduces the elasto-plastic deflection of the interface δ_{ep}. At this period, the plastic element acts against the elastic element ($d\delta_{ep}/dt < 0$), and the elasto-plastic element follows the unloading curve. Thus, some hysteresis loop is observed. Finally, the reloading from point D to point F follows the loading curve ($d\delta_{ep}/dt > 0$). This description clearly shows that the elasto-plastic element has three possible stages: $d\delta_{ep}/dt > 0$, $d\delta_{ep}/dt = 0$, and $d\delta_{ep}/dt < 0$. If m_{ep-e} and m_{ep-p} are equal, which makes the formulae simpler, then formula (2.3) can be written for the three stages as follows

$$\begin{aligned}
&\text{if} \quad \frac{d\delta_{ep}}{dt} > 0 \quad \text{then} \quad \delta_{ep} = e_{ep-l} p^{m_{ep}} \\
&\text{if} \quad \Big(\frac{\delta_{ep}}{e_{ep-e}}\Big)^{\frac{1}{m_{ep-e}}} + \Big(\frac{\delta_{ep}}{e_{ep-p}}\Big)^{\frac{1}{m_{ep-p}}} > p > \Big(\frac{\delta_{ep}}{e_{ep-e}}\Big)^{\frac{1}{m_{ep-e}}} - \Big(\frac{\delta_{ep}}{e_{ep-p}}\Big)^{\frac{1}{m_{ep-p}}} \\
&\quad \text{then} \quad \frac{d\delta_{ep}}{dt} = 0 \\
&\text{if} \quad \frac{d\delta_{ep}}{dt} < 0 \quad \text{then} \quad \delta_{ep} = e_{ep-unl} p^{m_{ep}}
\end{aligned} \tag{2.4}$$

where e_{ep-l}, e_{ep-unl} and m_{ep} denote the interface parameters. The contact pressure can be treated as the input signal, and then it governs the switching between the three stages. An example for the stage $d\delta_{ep}/dt = 0$ presents equation $(2.4)_2$. More information and pseudo-code are presented in the Appendix. The elasto-plastic module can be interpreted as a Hertz-Stajerman model (Michalczyk, 2008).

The contact model presented in Fig. 2a consists of three modules: plastic, elasto-plastic and elastic. Deflection of the model δ is the sum of three deflections given by

$$\delta = \delta_p + \delta_{ep} + \delta_e \tag{2.5}$$

where δ denotes the normal deflection of the contact. It is worth noting that the model have only seven parameters: e_e, e_p, m_e, m_p, e_{ep-l}, e_{ep-unl}, m_{ep}, and the contact behaviour described by the model is very similar to the experimental results (Fig. 2d). The loading from point A to point B (Fig. 2c) causes deflections of the three elements – plastic, elasto-plastic and elastic (Fig. 2b) – which indicates that the contact model is flexible (Fig. 2d). The unloading to point C changes the deflection in the elastic element only, whereas the unloading below point C reduces the deflection of the elasto-plastic element. The elasto-plastic element follows the unloading curve, Eq. $(2.4)_3$, at this time. During the reloading from point D to point E, the elastic and elasto-plastic elements are deflected together, and the elasto-plastic element follows the loading curve Eq. $(2.4)_1$. Exceeding the highest pressure so far, p_{max-B} at point E, makes the plastic deflection larger, and the contact becomes more flexible again. The three elements (modules) are then deflected together between points E and F. A similar sequence will be repeated during the next unloading-reloading cycle. The plastic nature of the dissipation is worth noting. It makes the model insensitive to the speed of deflection, because the damping force is insensitive to the magnitude of speed. This phenomenon is coupled with the insensibility of the dry contact hysteresis loops to the frequency of excitation (Gutowski and Skrodzewicz, 2001).

Table 1. The contact data used for the simulations

Parameters	Magnitudes of contact interface parameters	Units
e_p	0.534	$\mu\text{m}\,\text{MPa}^{-m_p}$
m_p	0.653	
e_e	1.148	$\mu\text{m}\,\text{MPa}^{-m_e}$
m_e	0.462	
e_{ep-l}	0.302	$\mu\text{m}\,\text{MPa}^{-m_{ep}}$
e_{ep-unl}	0.523	$\mu\text{m}\,\text{MPa}^{-m_{ep}}$
m_{ep}	0.462	

The parameters of the model, which are presented in Table 1, were estimated from experimental results (Tworzydlo *et al.*, 1998) using the Monte Carlo method. This method can be used to find the global minimum in a specific solution space. The contact pressure p was assumed to be an independent variable, whereas the contact deflection δ was assumed to be a dependent variable. The residual sum of squares was adopted as an objective function. Finally, the difference between the computational results and the experimental

results was minimised, which leads to a good agreement between the computational and experimental results (Fig. 2d).

Experimental investigations of the contact characteristics have been described previously in literature, see, e.g., Cichowicz and Nowicki (1984), Goerke and Willner (2008), Grudziński and Jaroszewicz (2002), Gutowski and Skrodzewicz (2001), Kostek (2005), Skrodzewicz (2003), Tworzydlo *et al.* (1998). The main difficulty associated with these investigations is the small contact deflection δ, which is a result of the small height of the roughness asperities. To overcome this difficulty, special displacement transducers are applied and special experimental setups are designed, or common testing machines are used. The experimental results used as a reference in this paper were obtained in Tworzydlo *et al.* (1998) for several disk specimens made of 1020 steel (Fig. 4). The thickness of the specimens was 3.175 mm and the diameter was 25.4 mm. The contacting surfaces of the specimens were glass-bead blasted, which introduced roughness. The standard deviation of the profile heights was $\sigma = 4.91\,\mu$m. A sandwich of the specimens was first loaded, then unloaded and finally reloaded. Recording the time histories of the loading force and contact deflection provides the opportunity to determine the contact characteristics. A more detailed description of the experimental setup and procedure can be found in Tworzydlo *et al.* (1998)

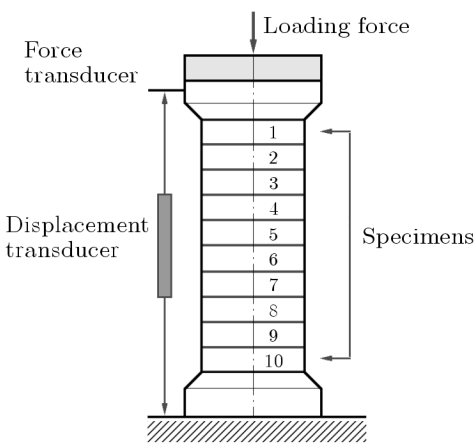

Fig. 4. Schematic of the experimental setup (Tworzydlo *et al.*, 1998)

3. Application examples

The model of contact presented in this paper, which was validated experimentally, has been applied to the modelling of interactions between rigid and elastic bodies. The parameters of the model are shown in Table 1. The first

example presents an interaction between rigid bodies that is typical for MBS systems. The second example presents the interaction between an elastic beam and a rigid flat. The last example presents the collision of elastics bodies that was simulated with the combined finite-discrete element method.

3.1. Rolling contact

A Hertzian contact is a classic issue in contact mechanics and tribology that is coupled with the coefficient of rolling friction and the deflection of contact. The model used for this case consists of a rigid cylinder rolling on a rigid flat (Fig. 5), and the elastic nature of the bodies is neglected (MBS). This model presents the influence of deflections of roughness asperities on the system. The contact zone has been modelled as a homogeneous layer, the constitutive relation of which has been described by the model presented here (Fig. 2). The contact pressure has been calculated for a number of points and then interpolated. In this way, the interaction between the bodies has been modelled.

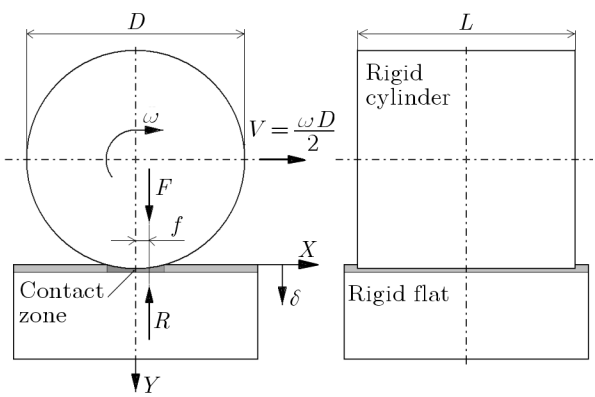

Fig. 5. Schematic of the rolling contact between a rigid cylinder and a rigid flat

During rolling, the contact zone is first loaded and then unloaded; the two stages of the process are presented in Fig. 6. The loading process and the unloading process follow different paths: the *A*-*B* characteristic during loading and the *B*-*C*-*D* characteristic during unloading (Fig. 2d), which introduces dissipation energy, rolling friction and residual deflection of contact δ_{pl} (Fig. 6a). The dissipation energy is coupled with the contact hysteresis (different loading and unloading characteristics). The amount of energy absorbed during loading is greater than the amount of energy released during unloading because of plastic deformation asperities. In other words, the area under the

loading characteristic is greater than the area under the unloading characteristic, which reflects the dissipation energy. The energy loss is proportional to the area of the hysteresis loop A-B-C-D-A.

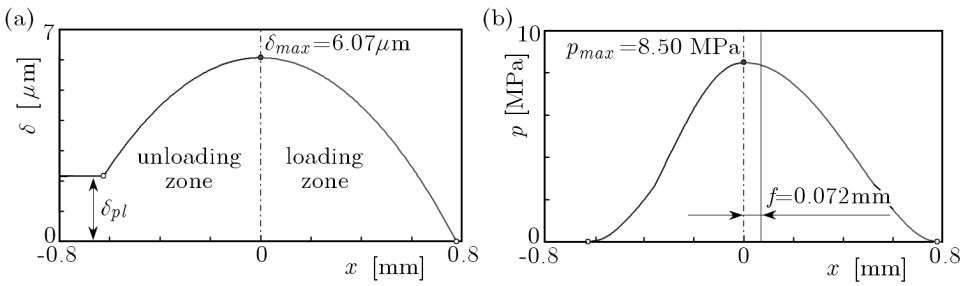

Fig. 6. Characteristics of the rolling contact (a) and contact pressure distribution (b) obtained for the following data: $D = 100\,\text{mm}$, $L = 100\,\text{mm}$, $F = 611.7\,\text{N}$

The resulting distribution of contact pressure is asymmetrical (Fig. 6b), which reflects contact hysteresis, dissipation energy and deformations of roughness asperities (Stolarski, 2000, p. 249). The asymmetry is a result of different loading and unloading characteristics. Thus, this model provides an opportunity to calculate the coefficient of rolling friction, which equals $f = 0.072\,\text{mm}$. "It is quite obvious that resistance to the rolling of a wheel is greater on a rough surface than on a smooth one, but this aspect of the subject has received little analytical attention" (Stolarski, 2000, p. 237).

The second issue is the contact deflection. For the contact interface described here, the maximum contact deflection equals $\delta_{max} = 6.07\,\mu\text{m}$ (Fig. 6a), which is over ten times more than the contact deflection resulting from a classical Hertzian contact of smooth bodies made of steel. As is evident from the results, the deflection of rough surfaces plays an important role in this system.

3.2. Prismatic beam on a rigid flat

The second example involves a cube-shaped elastic steel beam resting on a rigid flat surface and loaded by a force F (Fig. 7a). The elastic beam has been modelled with twenty beam elements (Young's modulus $E = 2 \cdot 10^5\,\text{MPa}$), which is a simplification of the model (Fig. 7b). The contact zone between the beam and the rigid flat has been modelled with the contact model presented in this paper (Table 1). The contact pressure p has been calculated for 21 nodes (Fig. 7b), and then the contact pressure distribution between the nodes has been interpolated with a linear function. Consequently, the distributed load q has been interpolated with a linear function as well (Fig. 7c). The loading

for a non-uniform space mesh can be calculated with this approach. Finally, the deflection of the beam due to contact pressure has been computed. The non-linearity of the contact presents some difficulties associated with the calculation of the contact pressure, which were solved with an iteration procedure and a gradual increase of the loading force F.

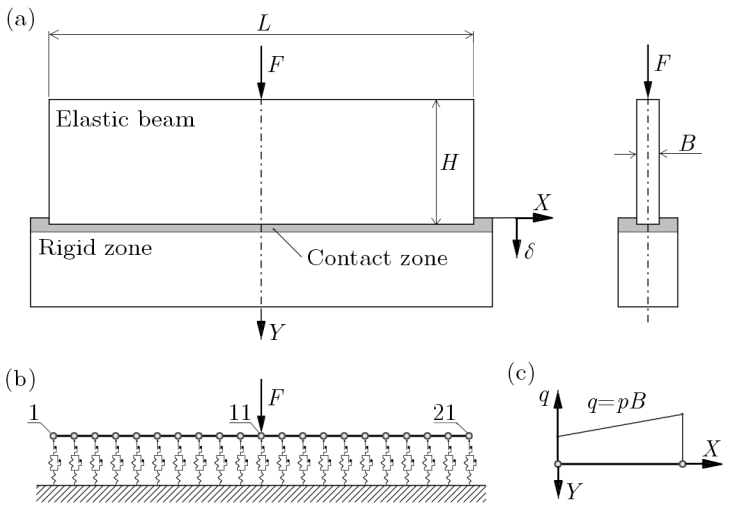

Fig. 7. Schematic of the contact interface between an elastic beam ($L = 200\,\text{mm}$, $B = 10\,\text{mm}$, $H = 62.4\,\text{mm}$) and a rigid flat (a), physical model of the interface (b), and interpolation of the load distribution between nodes (c)

The contact interface has been loaded, unloaded and reloaded, and a hysteresis of the interface has been obtained (Fig. 8). During the initial loading, the maximum pressure and contact deflection are observed in the middle of the interface (Fig. 9). As the loading force F increases and the beam distorts, the beam ends are gradually unloaded.

The unloading process is different from the loading process. The contact pressure in the middle part of the beam drops rapidly, which is a result of the plastic deflection of the contact. In turn, the beam ends are loaded during the unloading process. For a loading force of $F = 0.02\,\text{kN}$, the beam loses contact with the rigid flat (Fig. 10) in the middle part, and thus only the ends of the beam are loaded. Finally, for a loading force of $F = 0.00\,\text{kN}$ the contact is completely unloaded, and the residual (plastic) deflection of the contact is observed. The reloading process is very similar to unloading, but a higher force should be applied to cause the same contact deflections (Figs. 8, 10, and 11).

This model describes, for example, the contact pressure distribution within a screw joint. A similar model has been studied previously by researchers

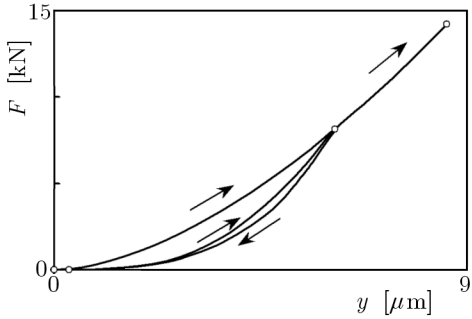

Fig. 8. A force-displacement characteristic of the contact interface and the displacement y of the 11th node against the loading force F

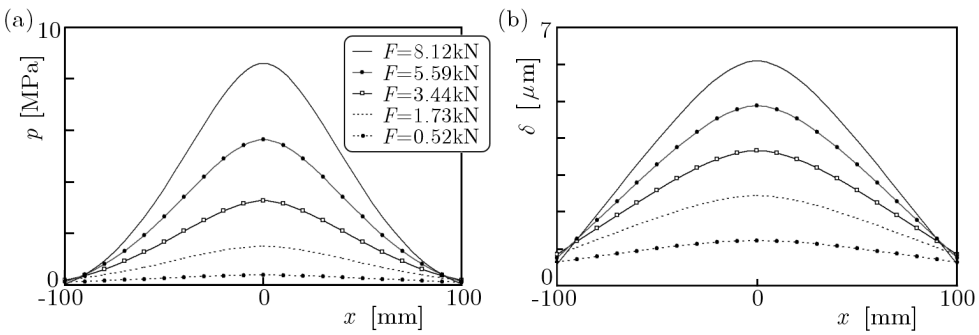

Fig. 9. The contact pressure distribution (a) and deflection of the contact (b) obtained for the initial loading

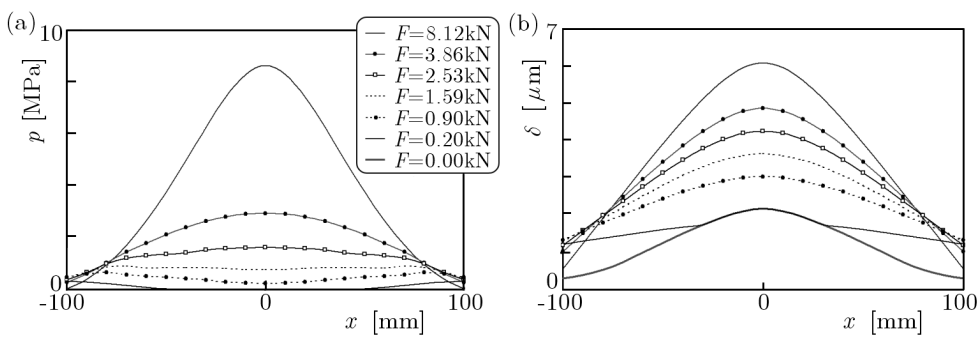

Fig. 10. The contact pressure distribution (a) and deflection of the contact (b) obtained for the unloading

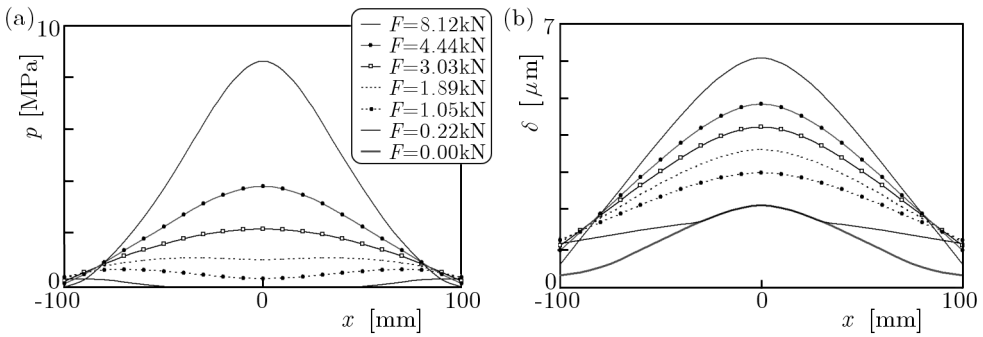

Fig. 11. The contact pressure distribution (a) and deflection of the contact (b) obtained for the reloading

(Buczkowski and Kleiber, 2006; Marshall *et al.*, 2006), but the issues of unloading and reloading in the normal direction have not been considered.

3.3. Collision of two elastic bodies

A collision between bodies is a classic issue in dynamics and is a problem that has been previously studied by many researchers. Interactions between bodies are usually described with simple models that reflect the restitution coefficient, but a collision is a far more sophisticated process. The kinetic energy of bodies can be dissipated by any of the following phenomena: plastic deflection of contact, plastic deformation of bodies, hysteresis of the material (internal friction), propagation of cracks, and the friction force between the bodies. Moreover, the impact can excite vibrations of the bodies, which reduce the restitution coefficient (see e.g. Lifshitz and Kolsky, 1963; Oden and Martins, 1985; Schiehlen *et al.*, 2006; Wriggers, 2006). These phenomena make the modelling of a collision difficult.

In this Section, the collision of two elastic bodies made of steel is studied (Young's modulus $E = 2.1 \cdot 10^{11}$ Pa, Poisson's ratio $\nu = 0.3$, density $\rho = 7860\,\mathrm{kg/m^3}$). The first body hits the second body with an initial velocity of $V_x = 0.5\,\mathrm{m/s}$, and the second body is fixed on one end (Fig. 12). Both bodies are modelled with FEM constant strain triangular elements (CSTE), the constitutive relation of which is described by Hooke's law for plane stress. All the FEM elements are equilateral triangles, and their masses are lumped into the nodes of the finite element mesh (node masses) (Munjiza, 2004) (Fig. 12). Thus, all acting forces are applied to the nodes. This approach leads to a number of second-order ordinary differential equations, which describe the dynamics of a point mass. This mass modelling technique provides an opportunity to

model the dynamics of two- and three-dimensional bodies (Stępniewski, 2007). The second body contains non-linear contact elements that model the contact zone and contact forces (Fig. 12). The normal forces are described with the contact model presented here, whereas the friction forces are described with the Coulomb model (coefficient of friction $\mu = 0.1$).

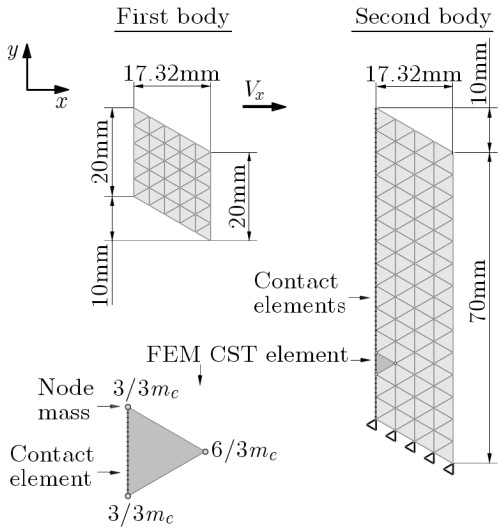

Fig. 12. The system of two bodies (before being collided) modelled with FEM constant strain triangular elements and contact elements; m_e – mass of FEM element

Each contact element contains twenty contact nodes. The contact nodes represent the contact of the roughness asperities, and so the contact forces are applied to the contact nodes (Fig. 13c). Normal and friction forces are calculated using a special procedure. The first stage of the procedure verifies if the individual edges of the bodies are close to each other (Fig. 13a). During this stage, the edges that are close to each other are selected, and the edges that are far from one another are eliminated. If the nodes of an edge and the nodes of the contact element are on the opposite sides of the line x_{min}, then they are not in contact (Fig. 13a). The selection process is performed for four lines: x_{min}, x_{max}, y_{min}, y_{max}, which eliminates most of the edges. The elimination process is a type of the bounding box method (Munjiza, 2004) and is based on conditional expressions, which makes the procedure fast to execute. The edges are then translated and rotated (Munjiza, 2004). Then, the procedure calculates the contact deflection (penetration) for each contact node (Fig. 13b). After this, the contact forces are calculated for each contact node (Fig. 13c)

from the velocities and positions of the contacting edges. Finally, the equivalent forces are applied to the nodes of the finite element mesh (Figs. 11b,c). This description is a brief summary of the main idea of the procedure. The modelling of the contact by contact nodes can be used when a non-uniform mesh is applied or when two bodies have a contact element.

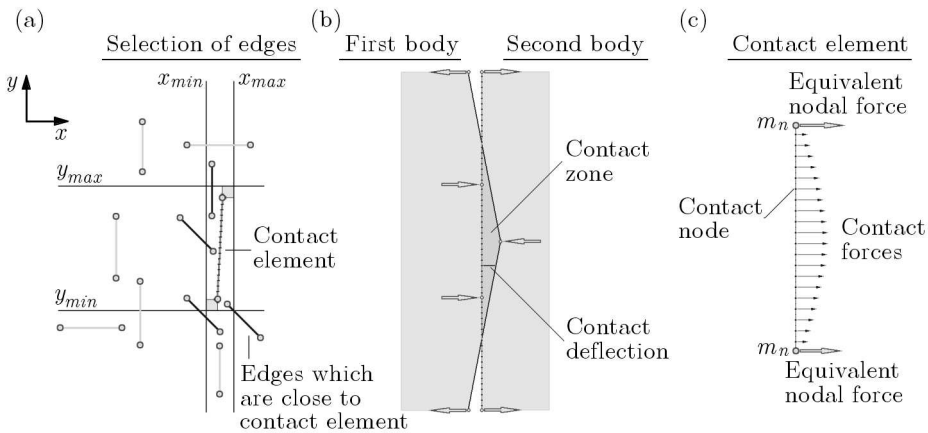

Fig. 13. Stages of the procedure for calculating contact forces: selection of edges (a), calculation of contact deflection (b), and calculation of contact and nodal forces (c)

The consecutive stages of the collision process are presented in Fig. 14. The initial velocity of the first body is $V_{x(t=0\mathrm{s})} = 0.5\,\mathrm{m/s}$ and $V_{y(t=0\mathrm{s})} = 0.00\,\mathrm{m/s}$. A stage before the initial contact is shown in Fig. 14a. Next, the magnitudes of the Hubert-Mises-Hencky effective stress of the elements that are near the contact zone gradually increases because of the increasing contact forces (Figs. 14a,b,c). The contact forces change the velocities of the first and second body at the same time (Figs. 14a,b,c). A part of the initial kinetic energy of the first body is transferred to the second body, after which the first body rotates (Fig. 14d). The contact zone has been loaded and unloaded during this period. The collision excites vibrations of the first body and the second body. The vibrations of the second body are presented in Figs. 14d,e,f, and Fig. 14g. The kinetic energy of the second body is converted to potential energy, which causes the second body to deflect (Figs. 14d,e,f). Thus, the velocity of the second body decreases, whereas the magnitude of the effective stress increases. The potential energy is then transformed into kinetic energy (Figs. 14f,g), which reflects the nature of vibrations. The two bodies are out of contact during this period. The average magnitudes of the velocity components of the first body are $\overline{V}_{x(t=9.4\cdot10^{-5}\mathrm{s})} = -1.25 \cdot 10^{-3}\,\mathrm{m/s}$ and $\overline{V}_{y(t=9.4\cdot10^{-5}\mathrm{s})} = 4.75\cdot10^{-2}\,\mathrm{m/s}$. It should be mentioned here that at this stage,

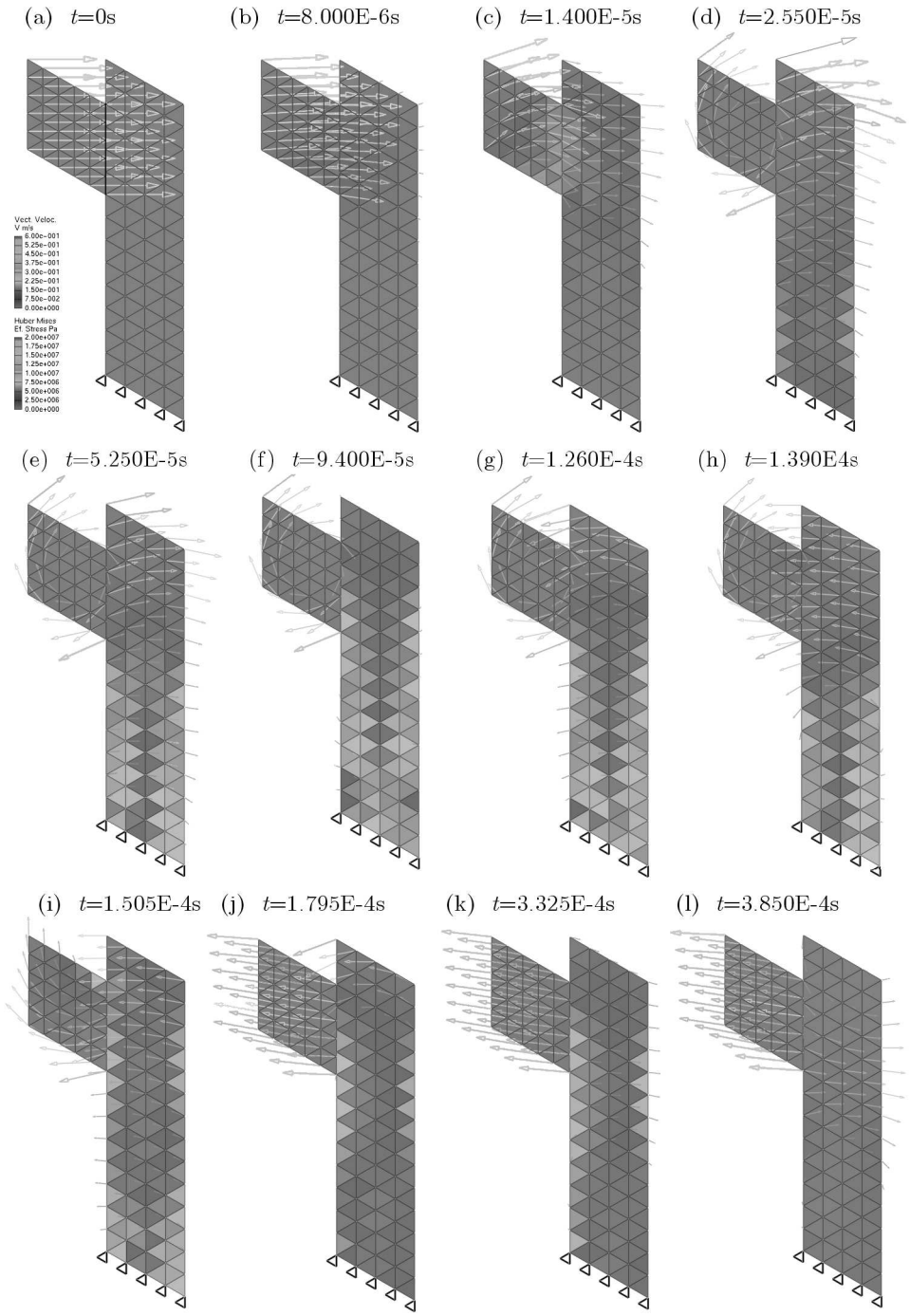

Fig. 14. Consecutive stages of collision presented for the time $t = 0\,\mathrm{s}$ (a) to $t = 3.850\mathrm{E}\text{-}4\,\mathrm{s}$ (l)

the y-component of the velocity is larger than the x-component. Finally, the second body hits the first body (Figs. 12h and i), which changes the velocity of the first body (Figs. 14h,i,j). The contact zone is reloaded and unloaded during this second collision. A part of the kinetic energy of the second body is transferred to the first body. After the second collision, the average magnitudes of the velocity components of the first body are $\overline{V}_{x(t=3.85\cdot10^{-4}\mathrm{s})} = -3.30 \cdot 10^{-1}\,\mathrm{m/s}$ and $\overline{V}_{y(t=3.85\cdot10^{-4}\mathrm{s})} = 5.15 \cdot 10^{-2}\,\mathrm{m/s}$. The vibrations of the bodies after collisions are presented in Figs. 12k,l. Only a part of the kinetic energy is returned to the first body. The initial energy excited vibrations of the bodies and has been dissipated in the contact zone. Moreover, the y-component of the velocity appears as a result of friction phenomena.

The results presented in this Section show the sophisticated nature of the collision process. Some simplifications used in the modelling of the collisions between the bodies, such as neglecting the deformations of the bodies or the application of simplified contact models, can lead to gross errors. The collision has been simulated and depicted using the proprietary programs FDEM_RK and DEV_KM (Kostek and Munjiza, 2009).

The visualization of the presented collision is available on the Internet http://www.youtube.com/watch?v=ql28X42P5D0.

4. Conclusions

A non-linear model of contact, which is dedicated especially to FEM, MBS and DEM, has been presented in this article. The model effectively demonstrates the contact characteristics, and it has a logical structure and a physical interpretation. The phenomena that occur in the contact are non-linear, which makes the modelling of contact difficult. This model adequately describes the following characteristic phenomena:

- the plastic deformation of a virgin contact,
- the hysteresis loop of a preloaded contact,
- the insensibility of the contact hysteresis to the frequency of loading.

The model is effective and accurate and has been validated experimentally.

Contact interfaces introduce plastic deflections, damping, hysteresis and memory of loading into many mechanical systems, which changes their stiffness, restitution coefficients and dynamical characteristics. Therefore, finding the relationship between the loading history and the deflection history seems to

be important. The model presented in this paper can be applied to the modelling of mechanical systems in which contact phenomena play a significant role, and can lead to the improved control of precision machines. Nowadays, a few microns of contact deflection are a significant factor for precision machining.

Appendix

This pseudo-code (Fig. 15) presents an algorithm which calculates the contact deflection δ from the contact pressure p. In this case, the contact pressure is the input signal, whereas the contact deflection is the output signal.

p, δ // input and output signals
p_{max}, δ_{ep} // variables which describe the inner state of the contact interface
// for virgin contact they are zero
$\delta_e = e_e p^{m_e}$; // elastic deflection
if $p > p_{max}$ then $p_{max} = p$ else $p_{max} = p_{max}$
$\delta_p = e_p p_{max}^{m_p}$; // plastic deflection
if $(\delta_{ep}/e_{ep-e})^{1/m_{ep-e}} + (\delta_{ep}/e_{ep-p})^{1/m_{ep-p}} > p >$
$> (\delta_{ep}/e_{ep-e})^{1/m_{ep-e}} - (\delta_{ep}/e_{ep-p})^{1/m_{ep-p}}$
then $d\delta_{ep}/dt = 0$; $\delta_{ep} = \delta_{ep}$; // elasto-plastic deflection, stick period

if $(\delta_{ep}/e_{ep-e})^{1/m_{ep-e}} + (\delta_{ep}/e_{ep-p})^{1/m_{ep-p}} < p$
then $d\delta_{ep}/dt > 0$; $\delta_{ep} = e_{ep-l} p^{m_{ep}}$; // elasto-plastic deformation, loading curve

if $p < (\delta_{ep}/e_{ep-e})^{1/m_{ep-e}} - (\delta_{ep}/e_{ep-p})^{1/m_{ep-p}}$
then $d\delta_{ep}/dt < 0$; $\delta_{ep} = e_{ep-unl} p^{m_{ep}}$; // elasto-plastic deformation, unloading curve

$\delta = \delta_p + \delta_{ep} + \delta_e$ // contact deflection – output signal

Fig. 15. The pseudo-code of the algorithm which calculates the contact deflection from the time history of contact pressure

If the contact deflection δ is the input signal, then the contact pressure p is the output signal. An algorithm, which solves this issue, is more complicated than that above presented. This problem can be solved with a iteration procedure, e.g. false position method, or Newton-Raphson method. A special procedure dedicated to this issue can be applied as well.

Acknowledgement

I would like to take the opportunity to thank W. Woytek Tworzydlo, Ph.D., Director, Research and Engineering, Altair Engineering, Inc. Austin, TX, for the experimental results.

References

1. Archard J.F., 1957, Elastic deformation and the laws of friction, *Proceedings of the Royal Society London, Ser. A*, **243**, 190-205
2. Buczkowski R., Kleiber M., 2006, Elasto-plastic statistical model of strongly anisotropic rough surfaces for finite element 3D-contact analysis, *Computer Methods in Applied Mechanics and Engineering*, **195**, 37/40, 5141-5161
3. Cichowicz M., Nowicki B., 1984, Contact stiffness and experimental investigations, *XIII Sympozjum Tribologiczne*, Częstochowa – Poraj, 316-321
4. Etsion I., Kligerman Y., Kadin Y., 2005, Unloading of an elastic-plastic loaded spherical contact, *International Journal of Solids and Structures*, **42**, 13, 3716-3729
5. Goerke D., Willner K., 2008, Normal contact of fractal surfaces-Experimental and numerical investigations, *Wear*, **264**, 7/8, 589-598
6. Greenwood J.A., Williamson J.B.P., 1966, The contact of nominally flat surfaces, *Proceedings of the Royal Society London, Ser. A*, **295**, 300-319
7. Grudziński K., Jaroszewicz W., 2002, *Posadowienie maszyn i urządzeń na podkładkach fundamentowych odlewanych z tworzywa EPY*, ZAPOL
8. Grudziński K., Kostek R., 2007, An analysis of nonlinear normal contact microvibrations excited by a harmonic force, *Nonlinear Dynamics*, **50**, 4, 809-815
9. Gutowski P., Skrodzewicz J., 2001, Experimental investigations of the planar contact joints under dynamic loads, *5th Conference on Experimental Methods in Designing and Maintenance Machines*, Wrocław University of Technology, Szklarska Poręba, **1**, 341-352
10. Hess D.P., Soom A., 1991, Normal vibrations and friction under harmonic loads: Part II – Rough planar contacts, *Transactions of the ASME, Journal of Tribology*, **113**, 1, 87-92
11. Hunt K.H., Crossley F.R.E., 1975, Coefficient of restitution interpreted as damping in vibroimpact, *Transactions of the ASME, Journal of Applied Mechanics*, **42**, 2, 440-445
12. Jamari J., Schipper D.J., 2007, Plastic deformation and contact area of an elastic-plastic contact of ellipsoid bodies after unloading, *Tribology International*, **40**, 8, 1311-1318
13. Jones R.E., 2004, Models for contact loading and unloading of a rough surface, *International Journal of Engineering Science*, **42**, 17/18, 1931-1947
14. Kadin Y., Kligerman Y., Etsion I., 2006, Unloading an elastic-plastic contact of rough surfaces, *Journal of Mechanics and Physics of Solids*, **54**, 12, 2652-2674

15. KIM J.Y., BALTAZAR A., ROKHLIN S.I., 2004, Ultrasonic assessment of rough surface contact between solids from elastoplastic loading-unloading hysteresis cycle, *Journal of the Mechanics and Physics of Solids*, **52**, 8, 1911-1934

16. KOSTEK R., 2005, Investigation of the normal contact microvibrations and their influence on the friction force reduction within the dynamical systems, Ph.D. Thesis, Technical University of Szczecin

17. KOSTEK R., KONOWALSKI K., 2008, A model of contact between rough surfaces, *Tribologia*, **39**, 5, 95-105

18. KOSTEK R., MUNJIZA A., 2009, Visualization of results received with the discrete element method, *Computational Methods in Science and Technology*, **15**, 2, 151-160

19. KRUGGEL-EMDEN H., WIRTZ S., SCHERER V., 2008, A study on tangential force laws applicable to the discrete element method (DEM) for materials with visco-elastic or plastic behaviour, *Chemical Engineering Science*, **63**, 6, 1523-1541

20. LI L.-Y., GU J.-Z., 2009, An analytical solution for the unloading in spherical indentation of elastic-plastic solids, *International Journal of Engineering Science*, **47**, 3, 452-462

21. LIFSHITZ J.M., KOLSKY K., 1963, Some experiments on anelastic rebound, *Journal of the Mechanics and Physics of Solids*, **12**, 1, 35-43

22. MARSHALL M.B., LEWIS R., DWYER-JOYCE R.S., 2006, Characterisation of contact pressure distribution in bolted joints, *Strain*, **42**, 1, 31-43

23. MARTINS J., ODEN J., SIMOES F., 1990, A study of static and kinetic friction, *International Journal of Engineering Science*, **28**, 1, 29-92

24. MICHALCZYK J., 2008, Phenomenon of force impulse restitution in collision modelling, *Journal of Theoretical and Applied Mechanics*, **46**, 4, 897-908

25. MIKIC B.B., 1971, Analytical studies of contact of nominally flat surfaces effect of previous loading, *Trans. ASME, Journal of Lubrification Technology*, **20**, 451-456

26. MIKIC B.B., 1974, Thermal contact conductance; Theoretical considerations, *International Journal of Heat and Mass Transfer*, **17**, 2, 205-214

27. MUNJIZA A., 2004, *The Combined Finite-Discrete Element Method*, John Wiley & Sons Ltd.

28. NARDIN A., ZAVARISE G., SCHREFLER B.A., 2003, Modelling of cutting tools-soil interactions – Part I: Contact behaviour, *Computational Mechanics*, **31**, 3/4, 327-339

29. NICOLA L., BOWER A.F., KIM K.-S., NEEDLEMAN A., VAN DER GIESSEN E., 2007, Surface versus bulk nucleation of dislocations during contact, *Journal of the Mechanics and Physics of Solids*, **55**, 6, 1120-1144

30. ODEN J.T., MARTINS J.A.C., 1985, Models and computational methods for dynamics friction phenomena, *Computer Methods in Applied Mechanics and Engineering*, **52**, 527-634

31. PEI L., HYUN S., MOLINARI J.F., ROBBINS M.O., 2005, Finite element modelling of elasto-plastic contact between rough surfaces, *Journal of the Mechanics and Physics of Solids*, **53**, 11, 2385-2409

32. POMBO J.C., AMBRÓSIO J.A.C., 2008, Application of a wheel-rail contact model to railway dynamics in small radius curved tracks, *Multibody System Dynamics*, **19**, 1/2, 91-114

33. PULLEN J., WILLIAMSON J.B.P., 1972, On the plastic contact of rough surfaces, *Proceedings of the Royal Society London, Ser. A*, **327**, 159-173

34. SCHIEHLEN W., SEIFRIED R., EBERHARD P., 2006, Elastoplastic phenomena in multibody impact dynamics, *Computer Methods in Applied Mechanics and Engineering*, **195**, 50/51, 6874-6890

35. SKRODZEWICZ J., 2003, Influence of the lubricating agent on the properties of contact joints, *Journal of Theoretical and Applied Mechanics*, **41**, 1, 107-118

36. STĘPNIEWSKI A., 2007, D'Alembert's supplemented principle and Newton's five supplemented laws, *International Journal of Pure and Applied Mathematics*, **38**, 3, 415-424

37. STOLARSKI T.A., 2000, *Tribology in Machine Design*, Elsevier

38. TWORZYDLO W.W., CECOT W., ODEN J.T., YEW C.H., 1998, Computational micro- and macroscopic models of contact and friction: formulation, approach and applications, *Wear*, **220**, 2, 113-140

39. VU-QUOC L., ZHANG X., 1999, An elastoplastic contact force-displacement model in the normal direction: displacement-driven version, *Proceedings – Royal Society. Mathematical, Physical and Engineering Sciences*, **455**, 1991, 4013-4044

40. WOO K.L., THOMAS T.R., 1980, Contact of rough surfaces: a review of experimental work, *Wear*, **58**, 2, 331-340

41. WRIGGERS P., 2006, *Computational Contact Mechanics*, 2nd Ed., Springer

Modelowanie charakterystyki kontaktu uzyskanej podczas obciążania odciążania oraz powtórnego obciążania

Streszczenie

W artykule przedstawiono nieliniowy matematyczny model opisujący histerezę suchego kontaktu ciał chropowatych, który został obciążony w kierunku normalnym. Kilka charakterystycznych zjawisk pojawia się podczas pierwszego obciążania, odciążania i powtórnego obciążania. Kontakt ciał jest najbardziej podatny podczas

pierwszego obciążania, a jego plastyczne odkształcenie jest znaczne. Natomiast charakterystyka uzyskana podczas odciążania jest sztywniejsza, a odkształcenia mają głównie charakter sprężysty. Podobną charakterystykę uzyskuje się podczas ponownego obciążania, tak więc obserwowana jest pewna pętla histerezy. Zweryfikowany doświadczalnie model kontaktu, opisujący wyżej wymienione nieliniowe zjawiska, został przedstawiony w artykule. Model ten został opracowany z myślą o: metodzie elementów skończonych, metodzie elementów dyskretnych i układach wieloczłonowych. W praktyce obliczeniowej potrzebne są dokładne modele kontaktu, które nie wymagają jednak kosztownych obliczeń. Prezentację tego modelu wzbogacono przykładami obliczeniowymi.

Manuscript received August 11, 2011; accepted for print September 30, 2011